PERGAMON

International Journal of Heat and Mass Transfer 45 (2002) 1445–1458

International Journal of HEAT and MASS TRANSFER

www.elsevier.com/locate/ijhmt

Falling-film and droplet mode heat and mass transfer in a horizontal tube LiBr/water absorber

Siyoung Jeong [1], Srinivas Garimella *

Department of Mechanical Engineering, Iowa State University, 2030 H.M. Black Engineering Bldg., Ames, IA 50011-2160, USA

Received 26 January 2001; received in revised form 14 July 2001

Abstract

A model for a horizontal tube absorber using LiBr/water as the working fluid was developed to predict heat and mass transfer in falling-film and droplet mode flow. In the analysis the effect of incomplete wetting is considered by introducing the wetting ratio. To validate the developed model a series of calculations is carried out under the same conditions as in experiments performed by other investigators. The simulation results for temperature, concentration variations, and heat and mass transfer rates are presented and compared with these experimental data. The effects of wetting ratio and solution flow rate on cooling capacity are discussed in detail.

1. Introduction

In recent years, absorption-cooling has drawn attention as an alternative to vapor compression cooling. The absorber is the most critical component of an absorption–cooling machine, and its characteristics have significant effects on overall system efficiency. The typical absorber of a conventional LiBr/water absorption–cooling machine consists of a bundle of horizontal tubes over which the absorbent solution is sprayed or distributed with drippers. The solution is introduced onto the tube as droplets or a sheet impinging on the top of a tube. After impingement, the solution spreads, flows around the tube as a film, and forms droplets on the underside of the tube. This type of falling-film absorber is used in most of the commercial machines because it has many advantages such as high heat transfer coefficient and low pressure drop. Theoretical and experimental research in the literature has attempted to describe the absorption mechanism and to develop optimal designs. However, commercial absorbers are still designed using empirical approaches because absorption phenomena are dependent on many parameters such as solution properties, solution flow rate, tube diameter, tube spacing, and surface wetting, which govern flow around and between the tubes. Therefore, simple smooth laminar falling-film models cannot predict absorber performance well, and it is realized that a reliable model for optimal design of absorbers will need to account for many of these factors.

2. Previous work

2.1. Experimental studies

Most of the experimental studies on LiBr/water horizontal tube absorbers have focused on measuring heat and mass transfer coefficients at different operating conditions. Dorokhov and Bochagov [1] suggested a simple experimental correlation over the entire range of actually encountered falling-film flow assuming a smooth, waveless, laminar film. Nomura et al. [2] performed a visualization study on an absorber using laser holographic interferometry and measured the solution temperatures on each tube surface and between the tubes. They found that the flow between tubes was in droplet mode and that the wetted surface area decreased gradually from upper to lower tubes. The average

* Corresponding author. Tel.: +1-515-294-8616; fax: +1-515-294-3261.

E-mail address: garimell@iastate.edu (S. Garimella).

[1] Permanent address: Department of Mechanical Engineering, Sogang University, CPO Box 1142, Seoul, Korea.

0017-9310/02/$ - see front matter
PII: S0017-9310(01)00262-9

Nomenclature

A	area (m^2)
c_1, c_2, c_3, and c_4	constants in Eqs. (3), (36) and (A.1) (dimensionless)
D	diffusivity (m^2/s)
d	diameter (m)
e_t	roughness of a tube (m)
f	friction factor (dimensionless)
g	gravitational acceleration (m/s^2)
Ga	Galileo number ($Ga = \rho\sigma^3/\mu^4 g$) (dimensionless)
h	specific enthalpy (J/kg)
h_i	heat transfer coefficient inside the tube (W/m^2 K)
h_o	film heat transfer coefficient (W/m^2 K)
K	mass transfer coefficient (m/s)
k	thermal conductivity (W/m K)
m	mass (kg)
$\dot{m}_s$	mass flow rate per unit length ($\dot{m}_s = \Gamma/2$) (kg/m s)
N	number of drops per unit tube length ($N = 1/\lambda$) (m^{-1})
n	exponent in Eq. (22) (dimensionless)
Nu	Nusselt number (dimensionless)
p	pressure (Pa)
Pr	Prandtl number ($Pr = \mu c_p/k$) (dimensionless)
q''	heat flux (W/m^2)
r	radius (m)
Re_i	Reynolds number inside a tube ($Re_i = \rho\bar{u}d_i/\mu$) (dimensionless)
Re_f	film Reynolds number ($Re_f = 4\dot{m}_s/\mu$) (dimensionless)
s	distance between tube rows (m)
T	temperature (°C)
t	time (s)
U	overall heat transfer coefficient (W/m^2 K)
u	velocity (m/s)
$\bar{u}$	average velocity (m/s)
w	width of falling-film flow (m)
WR	wetting ratio defined in Eq. (4) (dimensionless)
x	mass fraction of LiBr (%)
y	vertical distance from the surface of a tube (m)
δ_c	concentration boundary layer thickness (m)
δ_f	film thickness (m)
ϵ	ratio of concentration boundary layer thickness-to-film thickness ($\varepsilon = \delta_c/\delta_f$) (dimensionless)
λ	distance between droplets (m)
μ	dynamic viscosity (kg/m s)
ρ	density (kg/m^3)
σ	surface tension (N/m)
θ	angle from the top of a tube (rad)
ξ	capillary length ($\xi = \sqrt{\sigma/\rho g}$) (m)
η	vertical distance from the liquid/vapor interface (m)

Subscripts

a	attached half-spherical droplet
abs	absorption
b	core of the film
c	coolant
cen	center
cri	critical
d	detached spherical droplet
fall	droplet fall
film	falling-film
form	droplet-formation
i	interface, inside of a tube
o	outside of a tube
s	solution
t	top of the film
v	vapor
w	tube wall

wetting ratio could be as low as 0.5 in some cases. Another important result of their experiment was that the temperature of the solution between the tubes was higher than the solution temperature on the upstream tube surfaces. This indicates that a significant amount of vapor is also absorbed during the droplet-formation on the underside of a tube. Hoffman [3] also investigated heat transfer in a horizontal tube absorber with and without surfactants. He reported there was no simple correlation between film heat transfer coefficient and Reynolds number, which is different from the conclusions of other investigators. He concluded that the heat transfer coefficients increased with increasing mass flow and Reynolds number, but no well-defined relationship was found. He suggested that the influence of droplet-formation, fall and impingement had to be considered to obtain more realistic relationship. Wassenaar [4] measured heat and mass transfer in an absorber with 10 horizontal tubes. He also made visual observations on the wetted area, the flow pattern between the tubes, and the number of drainage sites. The film tended to break up in his experiments and he investigated several possible wettability criteria. He reported that wetting ratio is less than 100% if the surface tension gradient ($d\sigma/d\delta_f$)

is less than about 1. He also developed a model simplifying the absorber to a series of vertical falling films with mixing conditions in between. Recently, Deng and Ma [5] reported their experimental results on an absorber with 24 rows of tubes. They found that the heat transfer coefficient increased with inlet solution concentration and suggested a heat transfer relation including solution concentration as a parameter.

2.2. Analytical/numerical approaches

Most of the previous numerical studies have assumed that heat and mass transfer occur only in falling films, which are assumed to be laminar and wet the surface completely. Two studies by Nakoryakov and Grigoreva [6,7] considered the transfer of both heat and mass during the absorption of a vapor into a liquid film down a vertical wall. The authors assumed slug flow in the falling-film and noted that the temperature profile was linear over a large part of the film. Grossman [8] developed a model for absorption heat and mass transfer over an inclined flat plate. He considered absorption into laminar falling films for the case of constant temperature and an adiabatic wall. Andberg and Vliet [9,10] developed a model for absorption over horizontal tubes. They noted that concentration profiles exhibited a fair degree of similarity, but the temperature profiles did not. Kirby and Perez-Blanco [11] developed a model recognizing that the amount of vapor absorbed in flow regimes other than the falling-film regime might not be negligible. They identified three different flow regimes in their model: a falling-film region existing on a coolant tube, a region of drop formation on the under side of a tube, and a region of drop free fall between tubes. They considered the Reynolds number range $10 < Re < 100$ assuming that wetting is complete in this range and the flow is in droplet mode between tubes. However, in practical operation, wetting can be incomplete even in this range and the solution flow rate can be lower than $Re = 10$ in many cases.

From previous experimental studies on horizontal tube absorbers, it is realized that flow mode and the effect of wetting are very important in the analysis of the absorber. However, previous numerical models have not taken them into consideration. Therefore, in this study, the different modes of flow and incomplete wetting are taken into account to provide a more realistic description of the absorption process in horizontal tube absorbers.

2.3. Focus of present study

It is clear from the above discussion that most of the previous studies have evaluated absorber performance based primarily on overall heat balances and the refrigeration capacity of the entire absorber. However, to obtain a better understanding and to improve the performance of absorbers, it is necessary to evaluate the local heat and mass transfer rates at each tube. Local phenomena are analytically investigated in considerable detail in the present study. As a basis of comparison and model validation, the work of Nomura et al. [2], which reports absorption rates at individual tubes in a horizontal tube bank was selected, with the analytical models in the present study being developed for that geometry. Therefore, the absorber tested by them and also modeled here consists of 13 horizontal tubes that are used for commercial machines. Their measurements of temperatures on the tube surfaces as well as between the tubes, and conclusions about the effects of wetting of the tube surfaces, are compared with the results of the present modeling effort. To facilitate this comparison, operation conditions used in their study were also used as input parameters for the present work. Details of the geometry and operating conditions under consideration are provided in Table 1.

3. Modeling approach

The flow patterns established in an absorber are dependent on the solution mass flow rate. In most

Table 1
Absorber configuration and operating conditions [2]

Absorber configuration	Horizontal tube bank in counter flow (13 tubes) Tube size: 16 mm diameter bare tube Vertical pitch: 21 mm Tube length: 200 mm	
Operating conditions	Experiments of Nomura et al. [2]	Present study
Cooling water flow rate	0.0556 kg/s	0.0556 kg/s
Cooling water temperature	32 °C	32 °C
Solution flow rate	0.024–0.106 kg/m s	0.006–0.106 kg/m s
Solution inlet temperature	55 °C	Sub-cooled, $\Delta T_{sub} = 1$ K
Evaporating temperature	7.5–12.1 °C	6.0–12.0 °C

practical cases, the solution mass flow rate is usually maintained such that droplet flow exists between the coolant tubes. In this study, the three different flow regimes cited in the work of Kirby and Perez-Blanco [11] (falling-film region on the coolant tube, a region of drop formation on the under side of the tube, and a region of drop free fall between tubes) were considered. The solution passes through each of the three flow regimes in succession as it flows from one tube to the next tube. Because of the impingement of the droplet, complete mixing was assumed at the top of each tube. In all three regions, heat transfer to the vapor-side is neglected, based on an order of magnitude analysis. (See Appendix A.) Models for these regimes are discussed below.

3.1. Droplet flow and incomplete wetting

In their work on droplets and jets falling between horizontal tubes, Hu and Jacobi [12] suggested that the transition from droplet mode to jet mode occurred if Re_f is greater than the value given below:

$$Re_f = 4\dot{m}_s/\mu = 0.084Ga^{0.302}. \tag{1}$$

For a typical absorber design condition (60% LiBr/water solution at 40 °C), $Ga = \rho\sigma^3/\mu^4 g = 6.84 \times 10^7$. Therefore, the transition Re_f is about 19.5. A typical value of $\dot{m}_s$ is 0.01 kg/m s [10], which is equivalent to $Re_f = 6.2$. Therefore, the droplet mode should be assumed for such conditions. Hu and Jacobi [13] also reported the following relation for departure-site spacing between liquid droplets:

$$\lambda = \left(0.836\frac{2\pi\sqrt{3}}{\sqrt{1+2(\xi/d_o)^2}} - 0.863\frac{Re_f}{Ga^{1/4}}\right)\xi. \tag{2}$$

For a 60% LiBr/water solution at 40 °C, the capillary length ξ is about 2.3 mm and the spacing between droplets is about 18 mm for a conventional tube ($d_o = 16$ mm). Yung et al. [14] found from experiments that the diameter of a droplet just after it breaks off from the film may be expressed as follows:

$$d_d = c_1\xi. \tag{3}$$

The value of the constant c_1 was 3.0 with an uncertainty of ±5%.

As falling droplets impinge on the tube below, they will spread and flow down to the bottom of the tube. Since the diameter of a droplet is smaller than the droplet-site spacing for typical operating conditions, it is reasonable to assume that the tube may not be completely wet, depending on the extent to which the liquid spreads in a transverse direction on the tube surface. The shape of falling films formed on the tube surface depends on many parameters, such as flow rate of solution, tube diameter, distance between the tubes, fluid properties (including surface tension) which affect the droplet size and spacing, contact angles, and others. In this study, the flow is idealized by assuming that the width of the fluid film remains constant as the solution flows down, as shown in Fig. 1. The wetting ratio is defined as:

$$WR = \frac{A_{wet}}{A_{total}} = \frac{w}{\lambda}. \tag{4}$$

Since a reliable method to predict WR is not available at present, WR was used as a parameter in this study, and its influence was investigated numerically. If $WR = 1$, the problem is reduced to a more conventional analysis, in which the falling liquid film is evenly distributed over the entire tube surface.

3.2. Falling-film flow regime

As shown in Fig. 2, a fully developed laminar film is assumed and its flow characteristics are given by the well-known Nusselt equation [15]. The thickness and velocity of a falling-film are affected by wetting ratio, as shown in the following modified form of the Nusselt equation:

$$\delta_f = \left[\frac{3\mu\dot{m}_s}{(WR)\rho^2 g\sin\theta}\right]^{1/3}, \tag{5}$$

$$u = \frac{\rho g}{\mu}\left(\delta y - \frac{y^2}{2}\right)\sin\theta. \tag{6}$$

The average falling-film velocity is calculated as follows:

$$\bar{u} = \frac{\int_0^{\delta_f} u\,dy}{\delta_f} = \frac{\rho g\delta_f^2\sin\theta}{3\mu} = \frac{\dot{m}_s}{(WR)\delta_f\rho}. \tag{7}$$

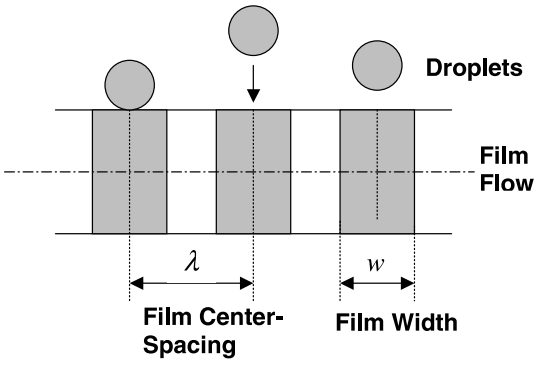

Fig. 1. Idealized falling-film flow with partial wetting.

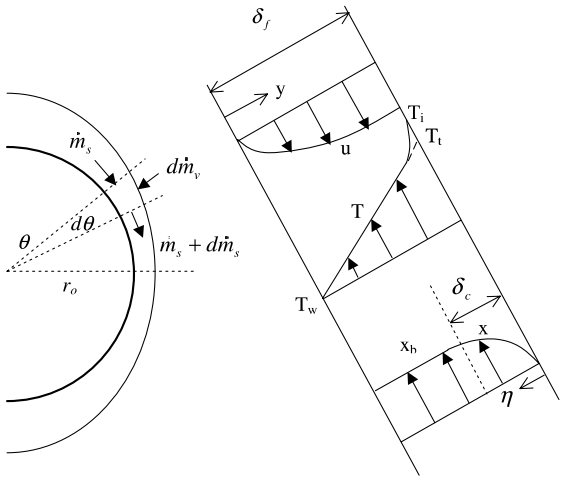

Fig. 2. Control volume for falling-film heat and mass transfer.

The total residence time of the falling-film is thus given by

$$t_{\text{film}} = \int \mathrm{d}t = \int_0^{\pi} \frac{r_o}{\bar{u}} \mathrm{d}\theta. \tag{8}$$

Assuming steady-state, the energy balance equation is as follows:

$$\dot{m}_s h_s + \mathrm{d}\dot{m}_s h_v = (\dot{m}_s + \mathrm{d}\dot{m}_s)(h_s + \mathrm{d}h_s) + U r_o \,\mathrm{d}\theta (T_s - T_c). \tag{9}$$

Since the specific enthalpy of the solution is a function of T_s and x_s, its differential is given by

$$\mathrm{d}h_s = \left.\frac{\partial h_s}{\partial T_s}\right|_{x_s} \mathrm{d}T_s + \left.\frac{\partial h_s}{\partial x_s}\right|_{T_s} \mathrm{d}x_s. \tag{10}$$

A concentration balance yields

$$\mathrm{d}\dot{m}_s = -\mathrm{d}x_s \frac{\dot{m}_s}{x_s}. \tag{11}$$

Substituting Eqs. (10) and (11) into Eq. (9), and dividing by $\mathrm{d}\theta$

$$h_{\text{abs}} \frac{\mathrm{d}\dot{m}_s}{\mathrm{d}\theta} - \dot{m}_s \left.\frac{\partial h_s}{\partial T_s}\right|_{x_s} \frac{\mathrm{d}T_s}{\mathrm{d}\theta} = U r_o (T_s - T_c), \tag{12}$$

where the heat of absorption is defined by

$$h_{\text{abs}} = h_v - h_s + x_s \left.\frac{\partial h_s}{\partial x_s}\right|_{T_s}. \tag{13}$$

In Eq. (12), the overall heat transfer coefficient is given by

$$U = 1 \Big/ \left\{ \frac{r_o}{r_i h_i} + \frac{r_o \ln(r_o/r_i)}{k_w} + \frac{1}{h_o} \right\}. \tag{14}$$

The Churchill equation [16] was used to calculate the heat transfer coefficient inside the tube.

Except for the region that is very close to the interface, a linear temperature profile was assumed across the film. Thus,

$$T = T_w + \frac{y}{\delta_f}(T_t - T_w). \tag{15}$$

In the above equation, T_t is the solution temperature very close to the interface, but it is different from interface temperature T_i. The departure from the linear behavior at the interface is due to the very high vapor absorption at this location.

The solution bulk temperature was calculated as follows:

$$T_s = \frac{\int_0^{\delta_f} Tu \,\mathrm{d}y}{\int_0^{\delta_f} u \,\mathrm{d}y} = \frac{\int_0^{\delta_f} Tu \,\mathrm{d}y}{\bar{u}\delta_f}. \tag{16}$$

Substituting Eqs. (6), (7), and (15) into Eq. (16) yields

$$T_s = \frac{5T_t + 3T_w}{8}. \tag{17}$$

Assuming that there is no heat transfer to the vapor, the heat of absorption is dissipated by conduction in the falling-film. Therefore,

$$q'' = \frac{k}{\delta_f}(T_t - T_w) = h'_o (T_s - T_w), \tag{18}$$

where h'_o is the film heat transfer coefficient without inclusion of the wetting ratio. From Eqs. (17) and (18)

$$h'_o = \frac{8}{5}\frac{k}{\delta_f}. \tag{19}$$

The actual solution-side heat transfer coefficient is obtained by including the wetting ratio as follows:

$$h_o = (WR) h'_o = \frac{8}{5}(WR)\frac{k}{\delta_f}. \tag{20}$$

In previous studies on LiBr/water absorption [6–10], it has been reported that the concentration profile develops much slower than temperature and velocity profiles. Therefore it is assumed that $\delta_c \ll \delta_f$. For convenience in the analysis, η is defined as the distance from the vapor–liquid interface. Then, from the following boundary conditions

$$\begin{aligned} &x = x_b \quad \text{at } \eta = \delta_c, \\ &\frac{\mathrm{d}x}{\mathrm{d}\eta} = 0 \quad \text{at } \eta = \delta_c, \\ &x = x_i \quad \text{at } \eta = 0 \end{aligned} \tag{21}$$

the concentration profile is expressed as follows:

$$x = x_b - (x_b - x_i)\left(1 - \frac{\eta}{\delta_c}\right)^n, \quad n > 1. \tag{22}$$

Based on an error function analysis, Andberg and Vliet [10] suggested $n = 2.33$. When diffusion takes place at

the tube wall, where axial and normal velocities are zero, $n = 2$ [17]. Because the calculation results were almost the same for $n = 2$ or 2.33, a parabolic concentration profile ($n = 2$) is assumed in the present study.

Since $\delta_c \ll \delta_f$, the entire concentration boundary layer is assumed to have interface velocity ($u = \rho g \delta_f^2 \sin\theta/2\mu$ for $0 < \eta < \delta_c$), and the interior concentration is equal to the inlet concentration for the particular tube under consideration ($x = x_b$ for $0 < y < \delta_f - \delta_c$). Then, the bulk concentration of the solution is calculated by integration across the film.

$$\begin{aligned} x_s &= \frac{(WR)}{\dot{m}_s}\int_0^{\delta_f} \rho u x \,\mathrm{d}y \\ &= \frac{\rho(WR)}{\dot{m}_s}\int_0^{\delta_c} \frac{\rho g \delta_f^2 \sin\theta}{2\mu}\left\{x_b - (x_b - x_i)\left(1 - \frac{\eta}{\delta_c}\right)^n\right\}\mathrm{d}\eta \\ &\quad + \frac{\rho(WR)}{\dot{m}_s}\int_0^{\delta_f-\delta_c} \frac{\rho g \sin\theta}{\mu}\left(\delta_f y - \frac{y^2}{2}\right)x_b \,\mathrm{d}y. \end{aligned} \tag{23}$$

Carrying out the integration, the following expression for the bulk concentration is obtained:

$$x_s = x_b - \frac{3}{2}\varepsilon\frac{(x_b - x_i)}{n+1}, \tag{24}$$

where $\varepsilon = \delta_c/\delta_f$. From Eqs. (11) and (24), the following relationship is obtained:

$$\begin{aligned} &[2(n+1)x_b - 3\varepsilon(x_b - x_i)]\frac{\mathrm{d}\dot{m}_s}{\mathrm{d}\theta} \\ &\quad + 3\dot{m}_s\left[\varepsilon\frac{\mathrm{d}x_i}{\mathrm{d}\theta} - (x_b - x_i)\frac{\mathrm{d}\varepsilon}{\mathrm{d}\theta}\right] = 0. \end{aligned} \tag{25}$$

The amount of vapor absorbed at the interface is given by following equation:

$$\begin{aligned} \frac{\mathrm{d}\dot{m}_s}{\mathrm{d}\theta} &= -\frac{\rho(r_o + \delta_f)(WR)D}{100}\left.\frac{\partial x}{\partial \eta}\right|_{\eta=0} \\ &= K_{film}\rho(r_o + \delta_f)\frac{(x_b - x_i)}{100}, \end{aligned} \tag{26}$$

where $K_{film} = n(WR)D/\delta_c$.

At the interface, the thermal equilibrium condition is assumed. Therefore,

$$p_v = p(x_i, T_i). \tag{27}$$

Because vapor pressure is kept constant during the process, the differential form of the above equation can be written as follows:

$$\left.\frac{\partial p}{\partial T_i}\right|_{x_i}\frac{\mathrm{d}T_i}{\mathrm{d}\theta} + \left.\frac{\partial p}{\partial x_i}\right|_{T_i}\frac{\mathrm{d}x_i}{\mathrm{d}\theta} = 0. \tag{28}$$

Although a linear temperature profile can be assumed for a large portion of the film, the temperature gradient at the interface is quite different from the average gradient across the film, especially in the initial flow regime. This is because the heat of absorption causes a steep temperature increase near the interface. As long as the exact temperature profile is not known, the boundary condition for the removal of the heat of absorption at the interface by heat conduction is not applicable. In view of this, as a first approximation, it is assumed here that the difference between the interface and bulk temperature remains constant as the solution flows over the tube

$$\frac{\mathrm{d}T_s}{\mathrm{d}\theta} - \frac{\mathrm{d}T_i}{\mathrm{d}\theta} = 0. \tag{29}$$

It is shown in a subsequent section of this paper that this assumption is reasonable in describing the falling-film absorption process over horizontal tube banks.

3.3. Solution method

For each calculation step of differential angle, five equations (Eqs. (12), (25), (26), (28), and (29)) with five unknowns ($\dot{m}_s$, T_s, T_i, x_i, and ε) are to be solved numerically. The set of differential algebraic equations was solved by using a DAE-solver, LSODI [18] (See Appendix B.) One half of the tube circumference ($0 \leqslant \theta \leqslant \pi$) was divided into 100 segments. The first and the last segment were excluded in the calculation, because the film thickness tends to infinity at $\theta = 0$ or $\theta = \pi$. Solution properties were assumed to be constant within a segment. Results from the analysis of each segment were used as inputs for the next segment. Because the DAE-system has five variables and each variable has its derivative, 10 initial conditions are required. Two of the initial conditions, the temperature and mass flow rate of solution ($\dot{m}_s$ and T_s), are given. It is assumed that the derivative of interface concentration is equal to zero ($\mathrm{d}x_i/\mathrm{d}\theta|_{\theta=0.01\pi} = 0$), and the initial value of ε is 0.001. Because initial conditions for the variables and the derivatives of the variables should satisfy the governing equations, the remaining six initial conditions are calculated from Eqs. (12), (25)–(29).

3.4. Droplet-formation regime

A detailed numerical study would be necessary to find the exact shape of the droplets formed on bottom of a tube. In this study, the shape of the droplet is idealized as a half sphere, as shown in Fig. 3. When the diameter of a droplet reaches the critical value ($d_{a,cri}$), it is detached from the tube. The critical diameter of the attached droplet is calculated by equating the volume of this half sphere to the falling spherical drop

$$d_{a,cri} = 2^{1/3} d_d. \tag{30}$$

The diameter of the falling spherical drop (d_d) is given by Eq. (3). The time required for droplet-formation (t_{form}) is calculated from continuity as follows:

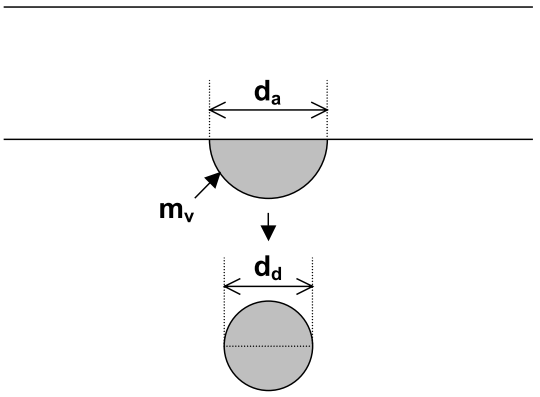

Fig. 3. Droplet-formation and fall shapes.

$$t_{\text{form}} = \frac{m_d N}{2\dot{m}_s}. \tag{31}$$

In the above equation, N is the inverse of λ in Eq. (2). The solution droplet (m_d) absorbs a small amount of vapor ($m_v = \Delta m_d$) in the droplet-formation stage. An adiabatic condition is assumed in this process. Considering the energy balance before and after the absorption process, the following equation is obtained:

$$m_d h_s + m_v h_v = (m_d + m_v)(h_s + \Delta h_s), \tag{32}$$

where

$$\Delta h_s = \left.\frac{\partial h}{\partial T_s}\right|_{x_s} \Delta T_s + \left.\frac{\partial h}{\partial x_s}\right|_{T_s} \Delta x_s.$$

A concentration balance yields

$$m_v = -\Delta x_s \frac{m_d}{x_s}. \tag{33}$$

Substituting Eq. (33) into Eq. (32), the following expression is obtained:

$$m_d \left.\frac{\partial h_s}{\partial T_s}\right|_{x_s} \Delta T_s = \left(h_v - h_s + x_s \left.\frac{\partial h_s}{\partial x_s}\right|_{T_s}\right) m_v. \tag{34}$$

From Eq. (13),

$$m_d \left.\frac{\partial h_s}{\partial T_s}\right|_{x} (T_{s,f} - T_{s,o}) = h_{abs} m_v. \tag{35}$$

In the above equation $T_{s,f}$ and $T_{s,o}$ are the solution temperatures after and before the vapor absorption.

Skelland and Minhas [19] compared mass transfer coefficients from different investigators in the form of the following equation:

$$K_{\text{form}} = c_2 \left[\frac{D}{\pi t_{\text{form}}}\right]^{1/2}. \tag{36}$$

In their work, the constant given by Heertjes et al. [20] ($c_2 = 24/7$) showed good agreement with experimental results. Heertjes et al. demonstrated the presence of internal circulation in rapidly growing drops ($t_{\text{form}} < 1.5$ s), and suggested this relationship for the case where the velocity of diffusion is small compared with the velocity of drop growth. In the present study, t_{form} is shorter than 1.5 s except for extremely low solution flow rates. Based on these considerations, the constant c_2 suggested by them was used here. The mass transfer coefficient used in this study was 2–3 times higher than those suggested by other investigators who did not consider internal circulation [19]. Due to this internal circulation, the temperature in the droplet was assumed to be uniform. Based on this mass transfer coefficient, the amount of vapor absorbed into a droplet during the formation stage is given by the following expression:

$$m_v = \rho K_{\text{form}} \frac{\pi}{2} d_a^2 t_{\text{form}} \frac{(x_{s,o} - x_{s,e})}{100}. \tag{37}$$

In the above equation, $x_{s,o}$ is the concentration of the solution flowing from the falling-film, and $x_{s,e}$ represents the equilibrium temperature at the given solution temperature and vapor pressure

$$p_v = p(x_{s,e}, T_s). \tag{38}$$

After calculating the absorbed vapor mass, the final droplet mass ($m_{d,f}$) is calculated by adding the absorbed vapor (m_v) to the initial droplet mass ($m_{d,o}$).

3.5. Droplet-fall flow regime

The droplet fall time is given by a simple free fall expression

$$t_{\text{fall}} = \sqrt{2s/g}. \tag{39}$$

The equations for the droplet free-fall flow regime were developed from a mass and energy balance on the falling droplet applying equations similar to those that were used for the droplet-formation regime. Thus,

$$\frac{dx_s}{dt} = -\frac{dm_d}{dt}\frac{x_s}{m_d}, \tag{40}$$

$$m_d \left.\frac{\partial h_s}{\partial T_s}\right|_{x} \frac{dT_s}{dt} = h_{abs} \frac{dm_d}{dt}. \tag{41}$$

The mass transfer in the droplet free-fall regime is determined by the following equation:

$$\frac{dm_d}{dt} = K_{\text{fall}} \rho 4\pi r_d^2 \frac{(x_s - x_i)}{100}. \tag{42}$$

In the above equation, the mass transfer coefficient given by Clift et al. [21] was used:

$$K_{\text{fall}} = 35\frac{D}{d_d}. \tag{43}$$

A linear temperature profile within the droplet was assumed to calculate the interface conditions:

$$T(r) = T_{cen} + \frac{(T_i - T_{cen})}{r_d} r. \quad (44)$$

This means that any internal circulation and convection was ignored. The solution bulk temperature was calculated by integrating this temperature profile as follows:

$$T_s = \frac{\int_0^{r_d} T 4\pi r^2 \, dr}{(4/3)\pi r_d^3} = \frac{T_{cen} + 3T_i}{4}. \quad (45)$$

Assuming once again that there is no heat transfer to the vapor, the heat of absorption is dissipated by conduction into the droplet, as shown below:

$$4\pi r_d^2 k \frac{(T_i - T_{cen})}{r_d} = h_{abs} \frac{dm_d}{dt}. \quad (46)$$

From Eqs. (45) and (46), the following equation is obtained:

$$T_i = \frac{h_{abs}}{16k\pi r_d} \frac{dm_d}{dt} + T_s. \quad (47)$$

Finally, thermal equilibrium is assumed at the interface

$$\left.\frac{\partial p}{\partial T_i}\right|_{x_i} \frac{dT_i}{dt} + \left.\frac{\partial p}{\partial x_i}\right|_{T_i} \frac{dx_i}{dt} = 0. \quad (48)$$

The five equations (Eqs. (40)–(42), (47), and (48)) for this regime with five unknowns (m_d, T_s, x_s, T_i, and x_i) were solved numerically using LSODI. The calculation was carried out using a time step of $t_{form}/100$.

4. Results and discussion

4.1. Local phenomena

Fig. 4 shows the variation of film thickness, bulk and interface temperatures and the relevant concentrations in the falling-film around the tube circumference for an intermediate solution flow rate ($\Gamma = 0.024$ kg/m s). Since the general trends were similar throughout the tube bank, the results are shown for the tube located in the middle of the tube bank (seventh tube from the top). This figure shows that the film is thicker near the top

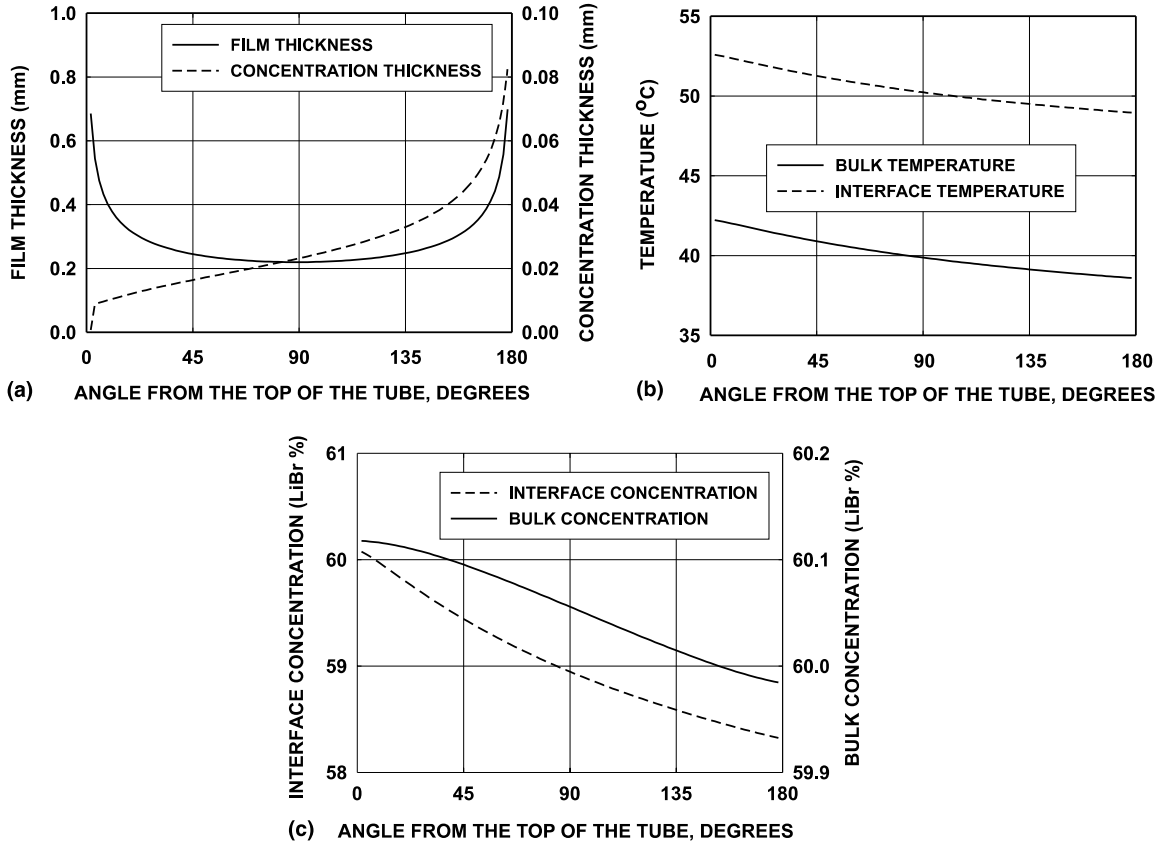

Fig. 4. Variations of: (a) film thickness, (b) temperature, and (c) concentration in the falling-film regime (seventh tube, $\Gamma = 0.024$ kg/m s, $T_E = 12$ °C, $WR = 0.8$).

and bottom of the tube, because the value of $\sin\theta$ in Eq. (5) approaches zero at $\theta = 0$ or 180°. The concentration boundary layer thickness increases almost linearly along the tube circumference. However, near the bottom of the tube, this increase is even steeper because the film becomes thicker and the solution velocity is lower in this region. The solution cools down as it flows over the tube. The bulk and interface temperatures vary in the same manner, as was assumed in Eq. (29). The change in interface concentration is about 10 times that of the bulk concentration. From the slope of the bulk concentration change, it is found that the vapor absorption rate at the top and bottom of the tube is low. Because the solution coming from the tube above has high temperature due to adiabatic absorption during the droplet-formation, the absorption process is slow at the top of the tube. Another reason for slow absorption is the increased film thickness at the top or bottom of the tube that makes the heat transfer coefficient lower. Andberg and Vliet [9] reported similar results in their work when the solution has a high inlet temperature.

Fig. 5 shows the variation of the droplet diameter, bulk and interface temperatures, and the relevant concentrations during the droplet-formation. The results shown here are also for the tube located in the middle of the tube bank (seventh tube from the top). Because the vapor mass absorbed is negligible compared to the droplet mass, the diameter of the droplet is almost proportional to the third power of the elapsed time. Vapor is absorbed rapidly at the beginning of the droplet-formation, and the absorption process slows down as the droplet grows. This rapid absorption of the vapor results in the steep decrease in the solution concentration and the steep increase in the bulk temperature. The interface temperature and concentration remain constant as were assumed.

In Table 2, the time interval, the mass transfer coefficient, and the increase in solution flow rate for each regime are compared. The time intervals for the falling-film and droplet-formation regime are about the same order of magnitude, while the time interval for droplet fall is much shorter. The mass transfer coefficient in the

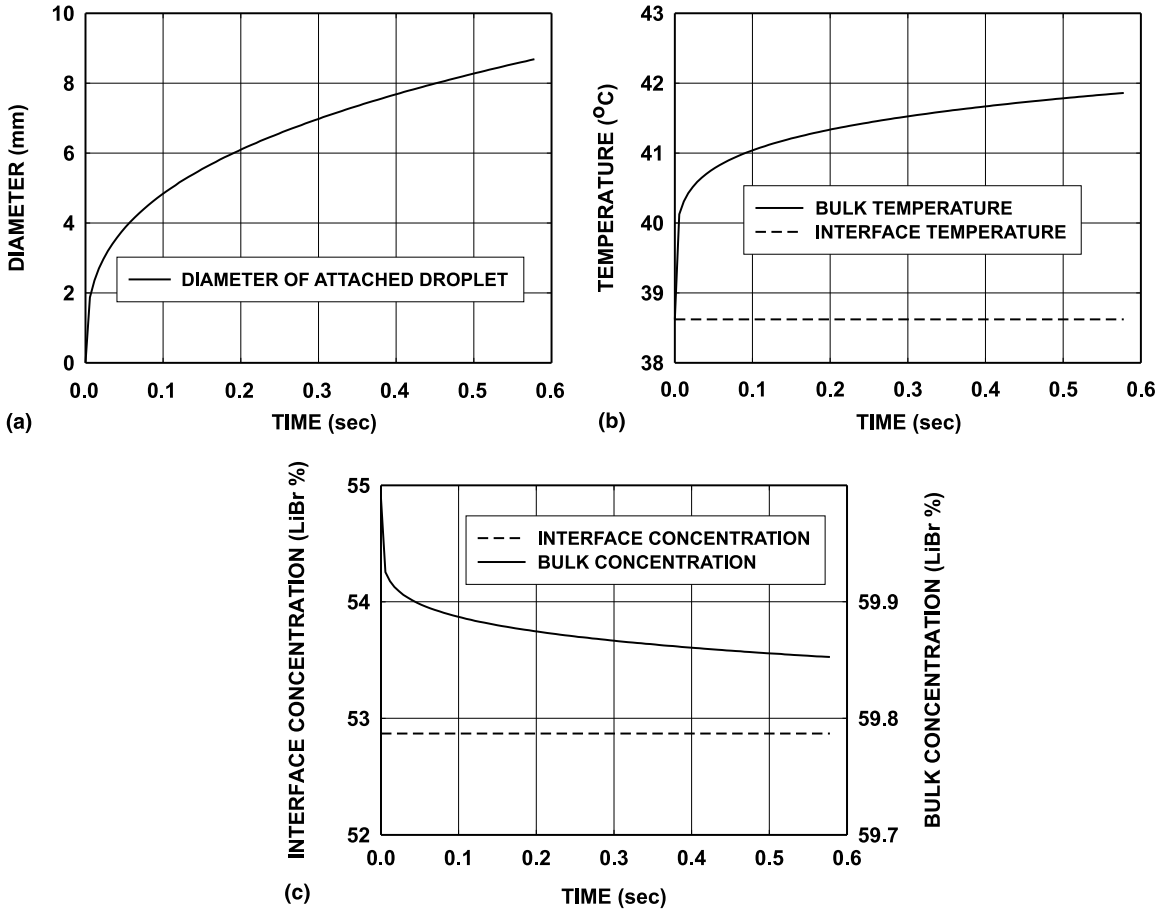

Fig. 5. Variations of: (a) diameter, (b) temperature, and (c) concentration in the droplet-formation regime (seventh tube, $\Gamma = 0.024$ kg/m s, $T_E = 12$ °C, $WR = 0.8$).

Table 2
Comparison of the three regimes (results for the seventh tube)

	Falling-film	Droplet-formation	Droplet fall
Time (s)	0.93	0.58	0.032
Mass transfer coefficient (m/s)	7.2×10^{-6} (90° from the top of the tube)	8.0×10^{-5} (at the end of droplet-formation)	5.1×10^{-6}
Increase in solution flow rate (kg/m s)	5.5×10^{-5}	5.7×10^{-5}	2.0×10^{-7}

Operating conditions: $\Gamma = 0.024$ kg/m s, $T_E = 12$ °C, $WR = 0.8$.

droplet-formation regime is higher than in the other regimes. It should be emphasized that the mass transfer coefficient used in the droplet-formation regime was based on the internal circulation model, which provides a higher mass transfer coefficient than other models without circulation. Because the change in the droplet-fall regime was found to be negligible, it is not shown separately, but included in the droplet-formation regime in the following results.

4.2. Variations over the tube bank

The solution experiences changes in three regimes as it flows down the tube bank. Because these changes are dependent on the solution flow rate, they are presented and discussed here for three different flow rates. A wetting ratio of 0.8 and an evaporating temperature of 12 °C were assumed for all three flow rates. All the other conditions are the same as shown in Table 1. At a low flow rate ($\Gamma = 0.006$ kg/m s) as shown in Fig. 6, the residence time is longer and the solution temperature change is greater. It is found that the tubes near the top absorb more vapor than the tubes at the bottom because of the large difference in the solution temperature and the coolant temperature near the top of the bank. Near the bottom, both the temperature difference and the available concentration gradient decrease, leading to lower absorption rates. It is also found that most vapor is absorbed in the falling-film region at this low solution flow rate, ranging from 86% of the total absorption rate for the first tube to 80% for the last tube in the bank. At low solution flow rates, the amount of vapor absorbed into a single droplet is greater; however, the frequency of droplet-formation is lower, the net result being lower absorption rates in the droplet-formation regime.

At intermediate solution flow rates ($\Gamma = 0.024$ kg/m s), about half of the vapor is absorbed in the droplet-formation regime (Fig. 7). In addition, after the first two tubes, the tubes show almost the same vapor absorption capability. At this flow rate, the solution does not lose much absorption capability as it flows down because the driving temperature difference between the solution and the coolant is essentially constant, and heat exchange takes place like in a balanced counter-flow heat exchanger.

Fig. 8 shows the high solution flow rate case ($\Gamma = 0.058$ kg/m s). The excellent agreement between the prediction and the experimental results of Nomura et al. [2] plotted in the figure shows that the model developed here describes the absorption process quite well. It can also be seen that the droplet-formation regime plays a more important role at higher flow rates. The frequency of droplet-formation is inversely proportional to the droplet-formation time. If other conditions are same, the absorbed mass for a droplet is proportional to the square root of the droplet-formation time. (See Eqs. (36) and (37).) Therefore, the vapor absorption rate in the droplet-formation regime is proportional to $1/\sqrt{t_{\text{form}}}$, or from Eq. (31), $\sqrt{\Gamma}$.

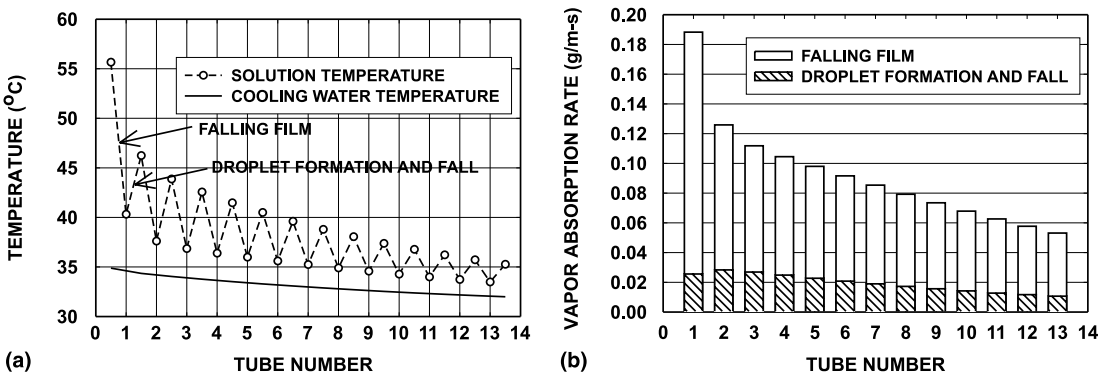

Fig. 6. (a) Temperature and (b) vapor absorption rate for low solution flow rate ($\Gamma = 0.006$ kg/m s, $T_E = 12$ °C, $WR = 0.8$).

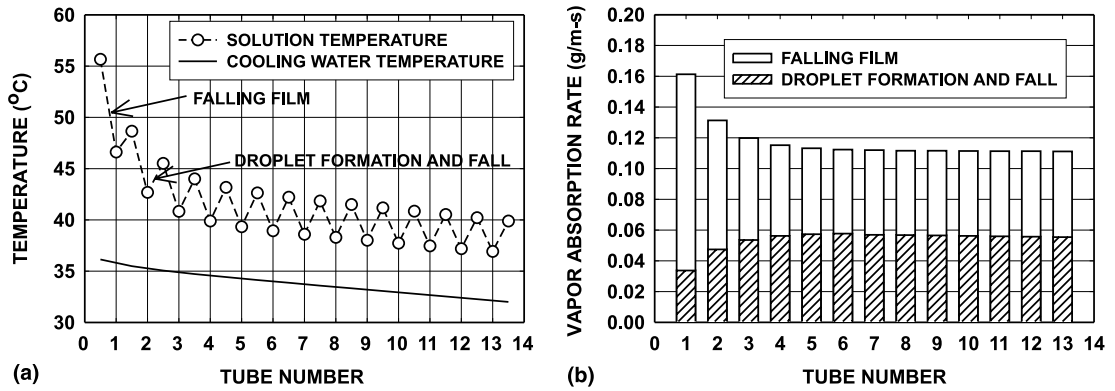

Fig. 7. (a) Temperature and (b) vapor absorption rate for intermediate solution flow rate ($\Gamma = 0.024$ kg/m s, $T_E = 12$ °C, $WR = 0.8$).

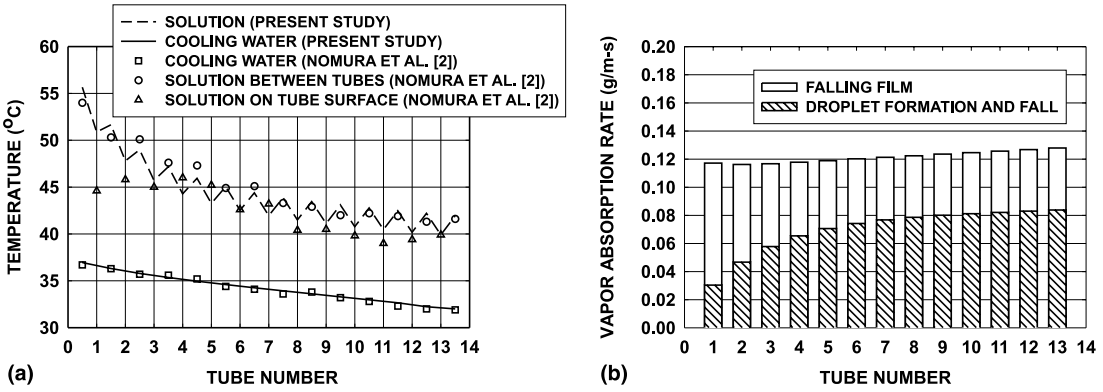

Fig. 8. (a) Temperature and (b) vapor absorption rate for intermediate solution flow rate ($\Gamma = 0.058$ kg/m s, $T_E = 12$ °C, $WR = 0.8$).

Fig. 9 shows the effect of wetting ratio on absorber performance. The results for wetting ratio of 0.4 and 0.8 are compared. For both cases, the evaporating temperature is 12 °C and Γ is 0.024 kg/m s. As the wetting ratio decreases, heat transfer and vapor absorption into the falling-film region are considerably reduced; however, at the same solution flow rate, vapor absorption into the droplet-formation region is not significantly affected by wetting ratio, essentially due to the independence of droplet-formation sites on wetting ratio.

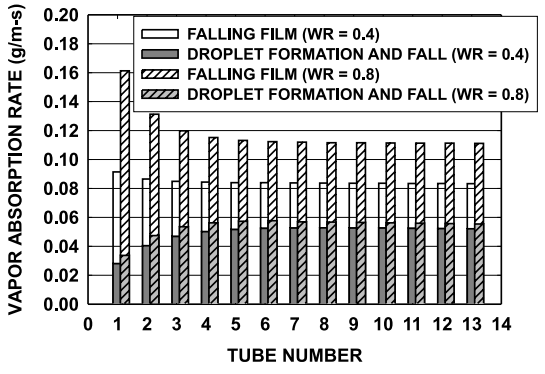

Fig. 9. Effect of wetting ratio on absorption rates ($\Gamma = 0.024$ kg/m s, $T_E = 12$ °C).

4.3. Overall performance

Fig. 10 shows the variation of cooling capacity with evaporating temperature and wetting ratio. The solution flow rate was kept constant ($\Gamma = 0.058$ kg/m s). Poor wetting can cause a large drop in performance. Nomura et al. [2] noted that wetting was not complete in their experiments. Based on the results shown in Fig. 10, most of their experiments seemed to have been carried out with a wetting ratio of 0.6 to 0.8. This illustration of the effects of wetting could explain the large variation in data from different experimental studies of absorption. It also appears from the data of Nomura et al. [2] that, at specific conditions, the wetting ratio could fluctuate considerably, which in turn causes the difference in capacity (Fig. 10, six data points near 9.3 °C).

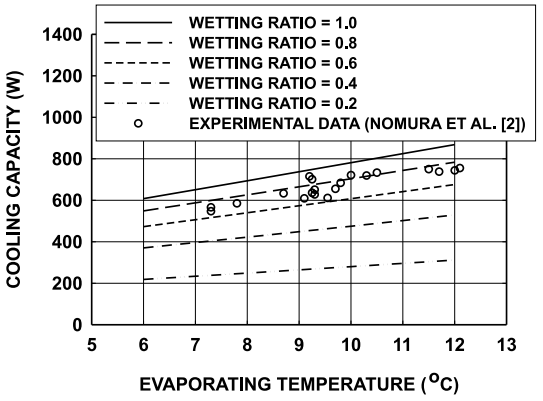

Fig. 10. Effect of evaporating temperature on cooling capacity ($\Gamma = 0.058$ kg/m s).

The effect of solution flow rate on cooling capacity and absorber heat load is shown in Fig. 11. It should be noted that the difference between cooling capacity and absorber heat load is the sensible heat load of the solution, which increases with solution mass flow rate. In this figure, it can be seen that absorber performance decreases sharply if the solution flow rate is smaller than 0.02 kg/m s. It can be also seen that absorber heat load increases with increasing solution flow rate; however, cooling capacity is not improved at solution flow rates higher than 0.04 kg/m s. Thus, only the sensible heat load component increases beyond a solution flow rate of about 0.04 kg/m s.

At the highest solution flow rate in the figure ($\Gamma = 0.106$ kg/m s), the cooling capacity at $WR = 0.2$ is about 31% of the cooling capacity at $WR = 1.0$. At the lowest solution flow rate ($\Gamma = 0.006$ kg/m s), this value increases to 55%. At high solution flow rates, the film heat transfer coefficient becomes low because of increased film thickness. If the wetting ratio is low at high solution flow rate, the film heat transfer coefficient becomes even lower. Therefore, the effect of wetting ratio on cooling capacity is more significant at higher solution flow rates.

In actual absorption machines, the wetting ratio becomes smaller with decreasing solution flow rate, and the experimental data of Nomura et al. [2] in Fig. 11 indicate this phenomenon clearly. Unfortunately, they did not report the results at solution flow rates less than 0.02 kg/m s; however, it is expected by extrapolating their data that the wetting ratio will decrease steeply at these flow rates. At lower wetting ratios, for example $WR = 0.2$, this figure shows that the cooling capacity decreases with increasing solution flow rate. In this case, the film heat transfer coefficient is greatly reduced due to the increased film thickness at these higher flow rates with low wetting ratios.

The variation of vapor absorption rate with wetting ratio is shown in Fig. 12. The evaporating temperature is 12 °C and Γ is 0.058 kg/m s. Vapor absorption in the falling-film regime is greatly affected by the wetting ratio because the effective heat and mass transfer area is directly proportional to wetting ratio. On the other hand, mass transfer in the droplet-formation regime is

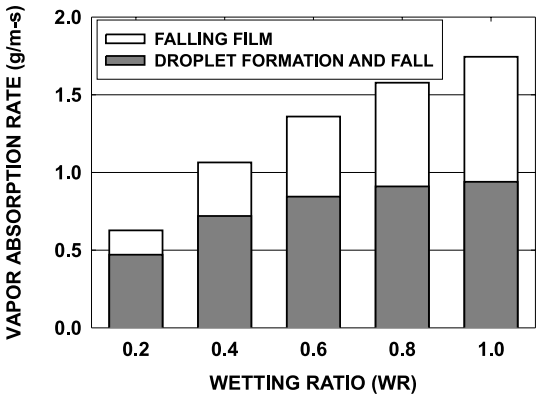

Fig. 12. Effect of wetting ratio on vapor absorption rate ($\Gamma = 0.058$ kg/m s, $T_E = 12$ °C).

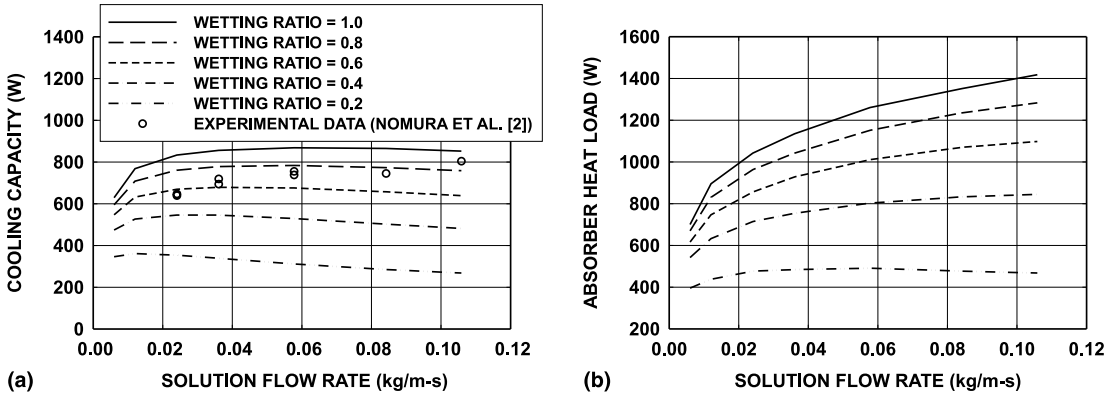

Fig. 11. Effect of solution mass flow rate on: (a) cooling capacity and (b) absorber heat load ($T_E = 12$ °C).

affected by the sub-cooling of the solution. At a higher wetting ratio, the solution is more sub-cooled in the falling-film regime because of better heat transfer, which makes the driving potential greater for mass transfer in the droplet-formation regime.

5. Conclusions

A comprehensive, flow mechanism-based model for the absorption of vapor in fluid pairs with non-volatile absorbents (LiBr/water) has been developed. This study represents one of the first efforts to accurately model absorption in the falling-film, droplet-formation, and droplet fall modes. In the analysis, the effect of incomplete wetting is addressed through the concept of wetting ratio. The governing equations are solved using a differential algebraic equation solver. Results from this model have been compared with experimental data from the literature and show excellent agreement over a wide range of operating conditions. Thus, the model successfully describes the actual absorption process in these different flow regimes. Specific conclusions are as follows:

- Vapor is absorbed mainly in the falling-film and droplet-formation regimes and heat and mass transfer in the free-fall regime is negligible.
- At low solution flow rates, the tubes near the top of the bank absorb more vapor than the tubes at the bottom, and more vapor is absorbed in the falling-film region than in the droplet-formation regime. As solution flow rate increases, the droplet-formation regime plays a more important role.
- Wetting ratio is significant in determining the performance of an absorber. The performance decreases rapidly at solution rates lower than 0.02 kg/m s because of poor wetting and a reduced available concentration gradient. For the configuration investigated, solution flow rates greater than 0.04 kg/m s do not improve cooling capacity, even though absorber load increases due to the sensible heat component.
- The importance of the droplet-formation regime, which was revealed by this study, points to the need for more detailed theoretical and experimental investigations of this regime.
- The effect of surfactants on wetting, heat and mass transfer are not considered in the present study, and further studies are required to understand their role in the absorption process.

Acknowledgements

The authors gratefully acknowledge support from the National Science Foundation through Grant Number 9875010 for this research.

Appendix A. Vapor-side heat transfer

The vapor-side heat transfer coefficient was estimated using the following heat transfer relation for tube banks in cross-flow [22]:

$$Nu_{\mathrm{d}} = c_3 Re_{\mathrm{d,max}}^{c_4} Pr^{0.36} \left(\frac{Pr}{Pr_{\mathrm{s}}} \right)^{1/4}. \tag{A.1}$$

In the above equation, $Re_{\mathrm{d,max}}$ represents the Reynolds number at the minimum cross-sectional area. Counter-flow was assumed for the solution and vapor, and the horizontal pitch of the tube bank was assumed to be the same as the vertical pitch (21 mm). The minimum width for vapor flow is 5 mm, because the diameter of the tube used is 16 mm. It was assumed that the effect of solution flow on the vapor flow was negligible and heat transfer occurred from the tube to the surrounding vapor. To calculate the $Re_{\mathrm{d,max}}$, the flow rate of the vapor for a representative operating condition was used. ($\dot{m}_{\mathrm{v}} = 2.83 \times 10^{-4}$ kg/s for $G = 0.057$ kg/m s, $WR = 0.8$, and $T_{\mathrm{E}} = 10$ °C.) All properties were evaluated for saturated vapor at 10 °C, except Pr_{s}, which was evaluated at the liquid–vapor interface temperature. At the resulting Reynolds number of 480, the Nusselt number was estimated to be 12, with the corresponding vapor-side heat transfer coefficient being 13 W/m^2 K, which is 1.7% of the liquid-side (including solution film, tube wall, and cooling water) heat transfer coefficient. The temperature difference between the vapor–liquid interface and vapor is greater than that between the interface and cooling water. Using these heat transfer coefficients and temperature differences, the vapor-side heat transfer rate was found to be about 3.7% of the total heat transfer rate. In actual absorption machines, the velocity of the vapor becomes smaller (heat transfer coefficient becomes lower) because of absorption, and the temperature of the vapor becomes higher (temperature difference becomes smaller), as it flows upward past the tubes. Therefore, the actual heat transfer to the vapor-side would be significantly smaller than the values calculated here. This estimate justifies the assumption of negligible interface-to-vapor heat transfer assumed in this study.

Appendix B. LSODI (Livermore solver for ordinary differential equations) [18]

LSODI solves the initial value problem for linearly implicit systems of first-order ordinary differential equations as follows:

$$\mathbf{a}(t, \mathbf{y}) \cdot \frac{\mathrm{d}y}{\mathrm{d}t} = g(t, y), \tag{B.1}$$

where $\mathbf{a}(t, \mathbf{y})$ is a square matrix. If $\mathbf{a}(t, \mathbf{y})$ is singular, this is a differential-algebraic system. To use the package, the

user should provide $\mathbf{a}(t,\mathbf{y})$ and $\mathbf{r}(t,\mathbf{y})$, the residual vector, defined as follows:

$$\mathbf{r}(t,\mathbf{y}) = g(t,y) - \mathbf{a}(t,\mathbf{y})\cdot\mathbf{s}, \tag{B.2}$$

where $\mathbf{s}$ is an internally generated approximation to $d\mathbf{y}/dt$.

The Jacobian matrix $d\mathbf{r}/d\mathbf{y}$ in closed form can also be supplied to improve calculation efficiency. If the initial value of $\mathbf{a}(t,\mathbf{y})$ is non-singular (and not too ill-conditioned), LSODI may compute the initial values of $\mathbf{y}$ and $d\mathbf{y}/dt$. If $\mathbf{a}(t,\mathbf{y})$ is initially singular, then the system is a differential-algebraic system, and the user must provide the initial values of $\mathbf{y}$ and $d\mathbf{y}/dt$. The accuracy of the solution is controlled by the relative and absolute tolerance parameters.

References

[1] A.R. Dorokhov, V.N. Bochagov, Heat transfer to a film falling over horizontal cylinders, Heat Transfer Soviet Res. 15 (2) (1983) 96–101.

[2] T. Nomura, N. Nishimura, S. Wei, S. Yamaguchi, Heat and mass transfer mechanism in the absorber of water/LiBr conventional absorption refrigerator: experimental examination by visualized model, in: International Absorption Heat Pump Conference, vol. 31, AES, American Society of Mechanical Engineers, New York, 1993, pp. 203–208.

[3] L. Hoffmann, Experimental investigation of heat transfer in a horizontal tube falling film absorber with aqueous solutions of LiBr with and without surfactants, Int. J. Refrig. 19 (5) (1996) 331–341.

[4] R.H. Wassenaar, Measured and predicted effect of flow rate and tube spacing on horizontal tube absorber performance, Int. J. Refrig. 19 (5) (1996) 347–355.

[5] S.M. Deng, W.B. Ma, Experimental studies on the characteristics of an absorber using $LiBr/H_2O$ solution as working fluid, Int. J. Refrig. 22 (1999) 293–301.

[6] V.E. Nakoryakov, N.I. Grigor'eva, Combined heat and mass transfer during absorption in drops and films, J. Eng. Phys. 32 (3) (1977) 243–247.

[7] N.I. Grigoryeva, V.E. Nakoryakov, Exact solution of combined heat and mass transfer problems during film absorption, J. Eng. Phys. 33 (5) (1977) 1349–1353.

[8] G. Grossman, Simultaneous heat and mass transfer in film absorption under laminar flow, Int. J. Heat Mass Transfer 26 (3) (1983) 357–371.

[9] J.W. Andberg, G.C. Vliet, Absorption of vapors into liquid films flowing over cooled horizontal tubes, in: Second ASME–JSME Thermal Engineering Joint Conference, vol. 2, 1987, pp. 533–541.

[10] J.W. Andberg, G.C. Vliet, A simplified model for absorption of vapors into liquid films flowing over cooled horizontal tubes, ASHRAE Trans. 93 (2) (1987) 2454–2463.

[11] M.J. Kirby, H. Perez-Blanco, A design model for horizontal tube water/lithium bromide absorbers, in: Heat Pump and Refrigeration Systems Design, Analysis and Applications, vol. 32, AES, American Society of Mechanical Engineers, New York, 1994.

[12] X. Hu, A.M. Jacobi, The inter tube falling film: Part 1 – flow characteristics mode transition and hysteresis, J. Heat Transfer 118 (1996) 616–625.

[13] X. Hu, A.M. Jacobi, Departure-site spacing for liquid droplets and jet falling between horizontal circular tubes, Exp. Thermal Fluid Sci. 16 (1998) 322–331.

[14] D. Yung, J.J. Lorenz, E.N. Ganic, Vapor/liquid interaction and entrainment in falling film evaporators, J. Heat Transfer 102 (1980) 20–25.

[15] W. Nusselt, Die oberflaechenkondensateion des wasserdampfes, Zeitschrift des Vereines Deutscher Ingenieur 60 (27) (1916) 541–546.

[16] S.W. Churchill, Comprehensive correlating equations for heat mass and momentum transfer in fully developed flow in smooth tubes, Ind. Eng. Chem. Fundam. 16 (1) (1977) 109–116.

[17] S. Sideman, H. Horn, D. Moalem, Transport characteristics of films flowing over horizontal smooth tubes, Int. J. Heat Mass Transfer 21 (1978) 285–294.

[18] J.F. Painter, A.C. Hindmarsh, Livermore Solver for Ordinary Differential Equations LSODI, Livermore National Laboratory, 1987.

[19] A.H.P. Skelland, S.S. Minhas, Dispersed phase mass transfer during drop formation and coalescence in liquid–liquid extraction, AlChE J. 17 (6) (1971) 1316–1324.

[20] P.M. Heertjes, W.A. Holve, H. Talsma, Mass transfer between isobutanol and water in a spray-column, Chem. Eng. Sci. 3 (1954) 122–142.

[21] R. Clift, J.R. Grace, M.E. Weber, Bubbles, Drops, and Particles, Academic Press, New York, 1978.

[22] A. Zhukauskas, Heat transfer from tubes in cross flow, in: J.P. Hartnett, T.F. Irvine Jr. (Eds.), Advances in Heat Transfer, Academic Press, New York, 1972.